Oxygen Reduction Reaction | Hot Paper

International Edition: DOI: 10.1002/anie.201804958
German Edition: DOI: 10.1002/ange.201804958

Efficient Oxygen Reduction Reaction (ORR) Catalysts Based on Single Iron Atoms Dispersed on a Hierarchically Structured Porous Carbon Framework

Zhengping Zhang, Junting Sun, Feng Wang, and Liming Dai**

Abstract: *Single Fe atoms dispersed on hierarchically structured porous carbon (SA-Fe-HPC) frameworks are prepared by pyrolysis of unsubstituted phthalocyanine/iron phthalocyanine complexes confined within micropores of the porous carbon support. The single-atom Fe catalysts have a well-defined atomic dispersion of Fe atoms coordinated by N ligands on the 3D hierarchically porous carbon support. These SA-Fe-HPC catalysts are comparable to the commercial Pt/C electrode even in acidic electrolytes for oxygen reduction reaction (ORR) in terms of the ORR activity ($E_{1/2}=0.81$ V), but have better long-term electrochemical stability (7 mV negative shift after 3000 potential cycles) and fuel selectivity. In alkaline media, the SA-Fe-HPC catalysts outperform the commercial Pt/C electrode in ORR activity ($E_{1/2}=0.89$ V), fuel selectivity, and long-term stability (1 mV negative shift after 3000 potential cycles). Thus, these nSA-Fe-HPCs are promising non-platinum-group metal ORR catalysts for fuel-cell technologies.*

To promote the large-scale application of fuel-cell technologies, cost-effective, high-performance non-platinum group metal (non-PGM) catalysts for oxygen reduction reaction (ORR) in both alkaline and acidic electrolytes have to be developed as alternatives to the precious and scarce Pt-based catalysts.[1–4] As one kind of non-PGM catalyst, Fe-based catalysts have been widely considered as a promising candidate to replace the Pt-based ORR catalysts. However, Fe-based catalysts still suffer from the poor electrochemical stability and unsatisfactory catalytic activity in acidic electrolyte.[5]

Along with the development of metal (e.g., Pt, Fe)-based nanoparticle catalysts, certain efficient Fe-based ORR catalysts with single-molecule or single-atom (SA) active sites have been studied.[3d,6] Although iron phthalocyanine (FePc), one of the most popular Fe-based molecular catalysts,[7] could facilitate the ORR process via a 4 electron pathway, demetalation of the catalytically active Fe atoms in FePc molecules was demonstrated to lead a rapidly declining activity.[5b,8] Besides, the inevitable Fenton reaction of Fe^{II} ions in $Fe^{II}Pc$ caused an instability in acidic electrolyte.[1,9] To eliminate the demetalation and/or degradation of molecular catalysts, it is highly desirable to develop SA-Fe catalysts, in which the coordinated Fe atoms are directly stabilized on carbon supports,[10] which can effectively prevent deactivation and facilitate electron transport. Recent studies demonstrated a few SA metal catalysts that are promising for energy-related electrocatalysis.[11,12] To date, the pyrolysis of precursors containing Fe, N, and C to generate unsaturated Fe atoms with N and C coordination (Fe-N/C) serves as one of the most important routes to Fe-N/C complex ORR catalysts.[13] To avoid the aggregation of Fe atoms and the loss of N-containing groups at high temperatures, the pyrolysis is performed in harsh atmospheres (e.g., NH_3), making it difficult to tailor the active sites and optimize the ORR performance by manipulating synthetic conditions.[12a,14] Therefore, direct pyrolysis of N-rich Fe precursors pre-supported on carbon substrates has recently attracted considerable attention to allow adequate control of the active-side structure.[14,15] However, it remains a challenge to develop desirable coordination environments for the Fe atoms in the carbon-supported Fe-containing precursors so as to avoid aggregation during pyrolysis.[5b,12a,15]

Herein, we choose hierarchically structured porous carbon (HPC) derived from biomass as the carbon support and iron phthalocyanine/unsubstituted phthalocyanine (FePc/Pc) complexes as the Fe precursors to fabricate the SA-Fe catalyst for ORR (Scheme S1 in the Supporting Information). To minimize the electrostatic interaction of Fe ions,[16] and hence isolation of Fe atoms, we intentionally add unsubstituted phthalocyanine (Pc) molecules to assemble with FePc molecules,[15b] through the π–π interaction of similar aromatic macrocyclic compounds, to provide a steric hindrance for Fe demetalation (Figure S1). Furthermore, the N-rich coordination structure in FePc/Pc complexes also facilitates the tuning coordination environment of Fe atoms during pyrolysis.[5b,15b,17] As we previously demonstrated, the HPC derived from cattle bones can provide various functional groups (e.g.,

[*] Dr. Z. Zhang, Dr. J. Sun, Prof. F. Wang
State Key Laboratory of Chemical Resource Engineering, Beijing Key Laboratory of Electrochemical Process and Technology for Materials
Beijing University of Chemical Technology
Beijing 100029 (China)
E-mail: wangf@mail.buct.edu.cn

Dr. Z. Zhang, Prof. L. Dai
Center of Advanced Science and Engineering for Carbon (Case4-carbon), Department of Macromolecular Science and Engineering
Case Western Reserve University
Cleveland, OH 44106 (USA)
E-mail: liming.dai@case.edu

Dr. Z. Zhang, Prof. F. Wang, Prof. L. Dai
Beijing Advanced Innovation Center for Soft Matter Science and Engineering, College of Energy
Beijing University of Chemical Technology
Beijing 100029 (China)

Supporting information and the ORCID identification number(s) for the author(s) of this article can be found under: https://doi.org/10.1002/anie.201804958.

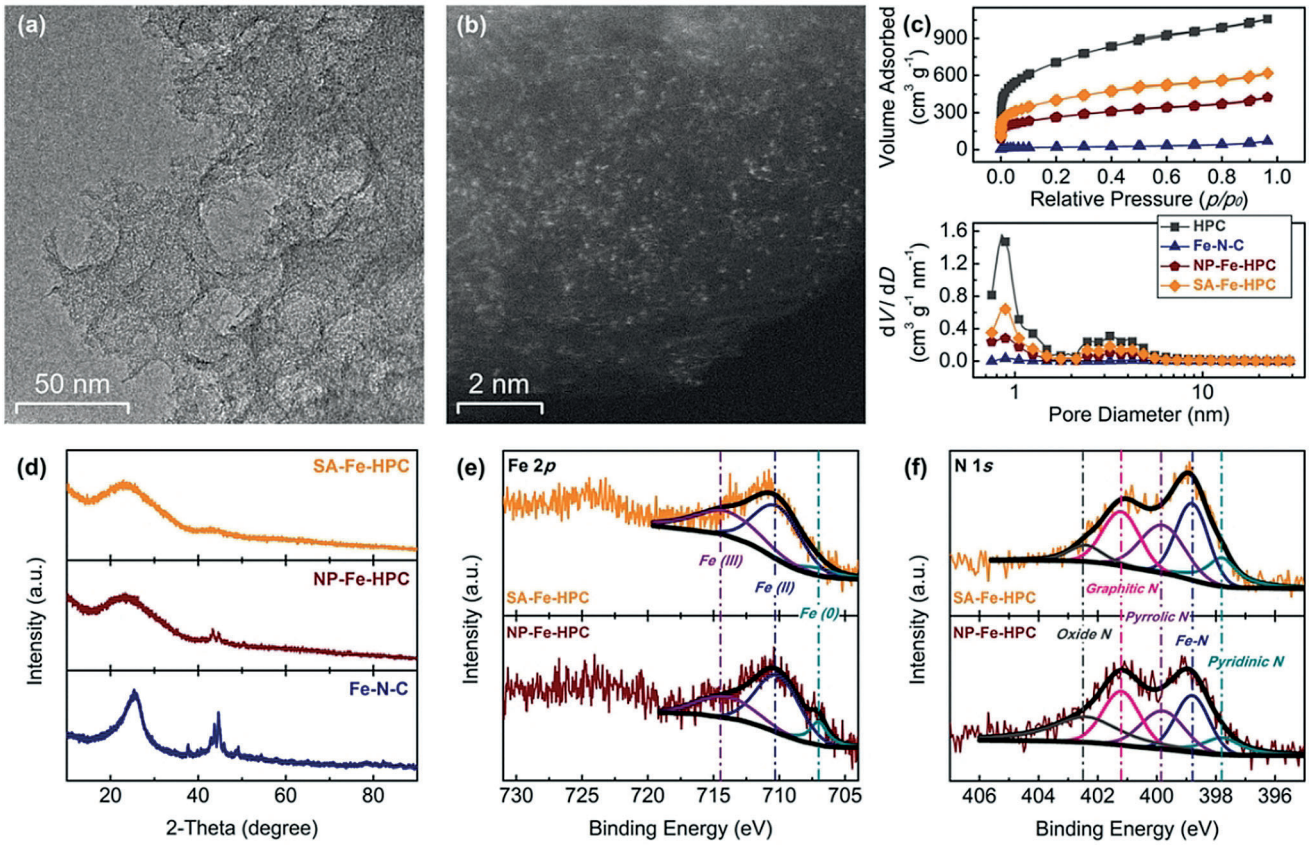

Figure 1. a) TEM and b) High-resolution HAADF-STEM images of the SA-Fe-HPC sample. c) BET characterization, nitrogen adsorption–desorption isotherms (top) and the corresponding DFT pore size distributions (bottom) of HPC, Fe-N-C, NP-Fe-HPC and SA-Fe-HPC. d) XRD patterns for Fe-N-C, NP-Fe-HPC and SA-Fe-HPC. High-resolution XPS spectra of e) Fe 2p and f) N 1s for NP-Fe-HPC and SA-Fe-HPC.

oxygen- and nitrogen-containing groups, Figure S2) and numerous micropores[18] to effectively confine and stabilize Fe atoms even during the optimized pyrolysis temperature of 800 °C (see, Figures S3, S4 and the synthetic optimization in Supporting Information) while its large surface area (2537.9 $m^2 g^{-1}$, Table S1) can increase the concentration/exposure of active sites. The same condition was used for the preparation of all other samples investigated in this study, including the HPC supported nanoparticle Fe (NP-Fe-HPC) and the conventional iron–nitrogen codoped carbon (Fe-N-C) electrocatalysts (see, Supporting Information).

Scanning electron microscopy (SEM) images of the SA-Fe-HPC show a 3D honeycomb porous structure similar to the open macropores (a diameter of ca. 500 nm of HPC (Figures S5a, S5d). The corresponding transmission electron microscopic (TEM) imaging revealed a channel mesoporous structure (ca. 30–50 nm) for the resultant SA-Fe-HPC without noticeable metal aggregation (Figure 1 a). To gain insights into the distribution of Fe atoms, we conducted the aberration-corrected high-resolution high-angle annular dark-field scanning transmission electron microscopic (HAADF-STEM) measurements on the SA-Fe-HPC sample. As shown in Figure 1 b, the single Fe atoms (the atomic scale of ca. 1 Å) are well-dispersed on the HPC support. Numerous micropores (< 1 nm) consisting of disordered carbon layers acted as anchor sites to stabilize the Fe atoms (Figures S6, S7). However, the control sample derived from the pure FePc-adsorbed HPC exhibited Fe aggregates on the HPC (designated as: NP-Fe-HPC), possibly formed during the high-temperature pyrolysis (Figures S5b, S8). Similarly, the conventional iron-nitrogen codoped carbon (Fe-N-C) produced by pyrolysis of commercial carbon black and pure FePc)[19] showed in homogeneously distributed Fe aggregates on the carbon substrate (Figure S5c).

The N_2 adsorption–desorption isotherm curves for all the as-prepared samples derived from HPC (i.e., HPC, SA-Fe-HPC and NP-Fe-HPC) displayed a similar I/IV-type isotherm characteristic of micro/mesoporous materials (Figure 1 c, top) Owing to the large surface area and high pore volume characteristics of HPC support (2537.9 $m^2 g^{-1}$ and 1.64 $cm^3 g^{-1}$), the SA-Fe-HPC (1436.3 $m^2 g^{-1}$ and 0.96 $cm^3 g^{-1}$) and NP-Fe-HPC (936.8 $m^2 g^{-1}$ and 0.66 $cm^3 g^{-1}$) exhibited a much larger Brunauer-Emmett-Teller (BET) surface area and higher total pore volume than those of the conventional Fe-N-C (68.5 $m^2 g^{-1}$ and 0.11 $cm^3 g^{-1}$). Compared to the HPC support, the SA-Fe-HPC and NP-Fe-HPC exhibited a decreased BET surface area attributable to the adsorption of FePc/Pc complex and pure FePc, respectively. The corresponding decrease in the nitrogen uptake ($p/p_0 <$ 0.1) for the SA-Fe-HPC and NP-Fe-HPC indicates that the

adsorption occurred mainly into the micropores.[17a] In view of the similar adsorption capacity and molecular size of iron phthalocyanine and unsubstituted phthalocyanine, we attributed the relatively small surface area of the NP-Fe-HPC with respect to that of the SA-Fe-HPC to the blockage of the pores and channels within the HPC support by Fe aggregates.[20]

In addition, we further conducted the density functional theory (DFT) calculations to predicate the pore size distribution (Figure 1c, bottom). It was found that all the samples derived from HPC possessed the hierarchical porous structure with micropores and small mesopores centered at 0.8 and 3.5 nm, respectively. In consistence with the decreased nitrogen uptake ($p/p_0 < 0.1$), the microporous surface area (S_{micro}) of the HPC decreased from 2076.2 $m^2 g^{-1}$ to 1089.9 $m^2 g^{-1}$ for SA-Fe-HPC and 752.6 $m^2 g^{-1}$ for NP-Fe-HPC by Fe adsorption. Compared with the mesoporous surface area (S_{meso}) of HPC (461.7 $m^2 g^{-1}$), the SA-Fe-HPC showed a similar S_{meso} (346.4 $m^2 g^{-1}$) whilst an obviously decreased S_{meso} (184.2 $m^2 g^{-1}$) was observed for NP-Fe-HPC due, most probably, to the blockage associated with the Fe aggregates.[21]

To measure the iron and carbon crystalline structures, we further performed powder X-ray diffraction (XRD). The SA-Fe-HPC and NP-Fe-HPC showed a broad diffraction peak around 23.1° (Figure 1d) corresponding to C(002) with a low-angle-shift in respect to the commercial graphitic carbon (26.4°).[22] Apart from the broad C(002) peak, the SA-Fe-HPC did not show any characteristic peak for metallic iron, iron nitrate or iron carbide crystals. In contrast, the Fe-N-C exhibited a set of sharp peaks (37.7°, 43.7°, 44.9°, and 48.6°) characteristic of iron carbide (JCPDS card: no. 35–0772). It is worth to note that the NP-Fe-HPC sample also exhibited a few small, but noticeable, characteristic peaks at 43.7° and 44.9°, though its microporous structure could stabilize Fe atoms and confine Fe aggregates. Furthermore, Raman spectrum of the NP-Fe-HPC showed a higher graphitization degree with a higher G band to D band ratio (I_G/I_D, ca. 0.91) than those of the HPC and SA-Fe-HPC (ca. 0.84) due probably to additional graphitization induced by Fe nanoparticles during the high temperature pyrolysis (Figure S9).

We have further carried out X-ray photoelectron spectroscopic (XPS) measurements on HPC, SA-Fe-HPC and NP-Fe-HPC. The XPS survey spectra (Figure S10a, Table S2) indicate that all the samples are dominated by carbon, along with some nitrogen and oxygen-containing moieties, while the SA-Fe-HPC and NP-Fe-HPC samples show the presence of Fe (0.80 and 0.45 at%, respectively). The corresponding high-resolution XPS spectra of Fe $2p_{3/2}$ (Figure 1e, Table S3) were deconvoluted into three component peaks at 707.1, 709.0 and 714.0 eV,[12b,13b] arising from the metallic iron, ferrous state, and ferric state, respectively. Fe^{II} and Fe^{III} species were observed for both SA-Fe-HPC and NP-Fe-HPC. However, Fe^0 was observed only for the NP-Fe-HPC sample, indicating, once again, the presence of the Fe aggregates. In view of the different Fe^{III}/Fe^{II} ratios in SA-Fe-HPC (0.71) and NP-Fe-HPC (0.49), we further deconvoluted the high-resolution XPS N 1s spectra (Figure 1f) into five component peaks at 397.7, 398.7, 399.8, 401.2 eV, and 402.4 eV corresponding to pyridinic N, Fe–N bonding, pyrrolic N, graphitic N and oxide N (Figure 1f), respectively.[22] Compared to the deconvoluted high-resolution XPS N 1s spectrum of HPC (Figure S10b), it is believed that the graphitic N and oxide N species in the SA-Fe-HPC and NP-Fe-HPC are mainly originated from the N-doped carbon skeletons in HPC (Table S4). Compared to NP-Fe-HPC, the relatively high contents of pyridinic N, Fe–N bonding, and pyrrolic N observed for SA-Fe-HPC indicate the presence of more N ligands.

To confirm the presence of single dispersed Fe atoms, we further performed the X-ray absorption near-edge structure (XANES) and extended X-ray absorption fine structure (EXAFS) measurements. As seen in Figure 2a, the XANES spectrum of SA-Fe-HPC shows the Fe K-pre-edge close to that of the unpyrolyzed $Fe^{II}Pc$. However, the absence of the pre-edge peak at 7118 eV from SA-Fe-HPC revealed that the square-planar D_{4h} local symmetry of FePc was broken after the pyrolysis treatment.[23] In contrast, the XANES spectrum of NP-Fe-HPC is more similar to that of Fe foil, indicating the presence of metallic Fe^0 nanoparticles in the former. Furthermore, the SA-Fe-HPC exhibited higher half-edge energy than that of NP-Fe-HPC due to a negative charge transfer from iron to nitrogen.[24] These results are consistent with the XPS data.

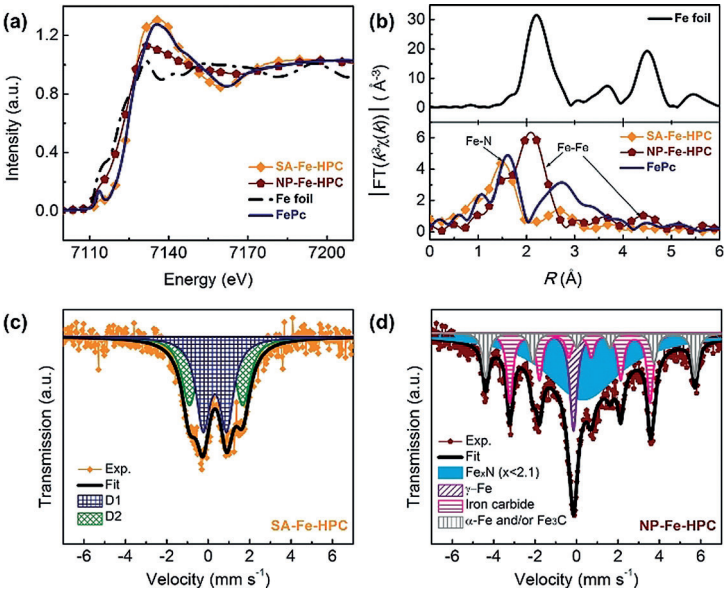

Figure 2. a) Fe K-edge XANES spectra and b) Fourier transforms of k^3-weighted $\chi(k)$-function of the EXAFS spectra for the SA-Fe-HPC and NP-Fe-HPC samples with iron foil and FePc as references. The ^{57}Fe Mössbauer transmission spectra measured at 293 K for c) SA-Fe-HPC and d) NP-Fe-HPC.

To gain further structural information about Fe atom, we carried out Fourier transformed EXAFS spectroscopic measurements (R space) on the SA-Fe-HPC and NP-Fe-HPC samples. As can be seen in Figure 2b, the SA-Fe-HPC exhibited a slight shift in the Fe-N (1.5 Å) coordination peaks compared to Fe atom with four-coordinated nitrogen in

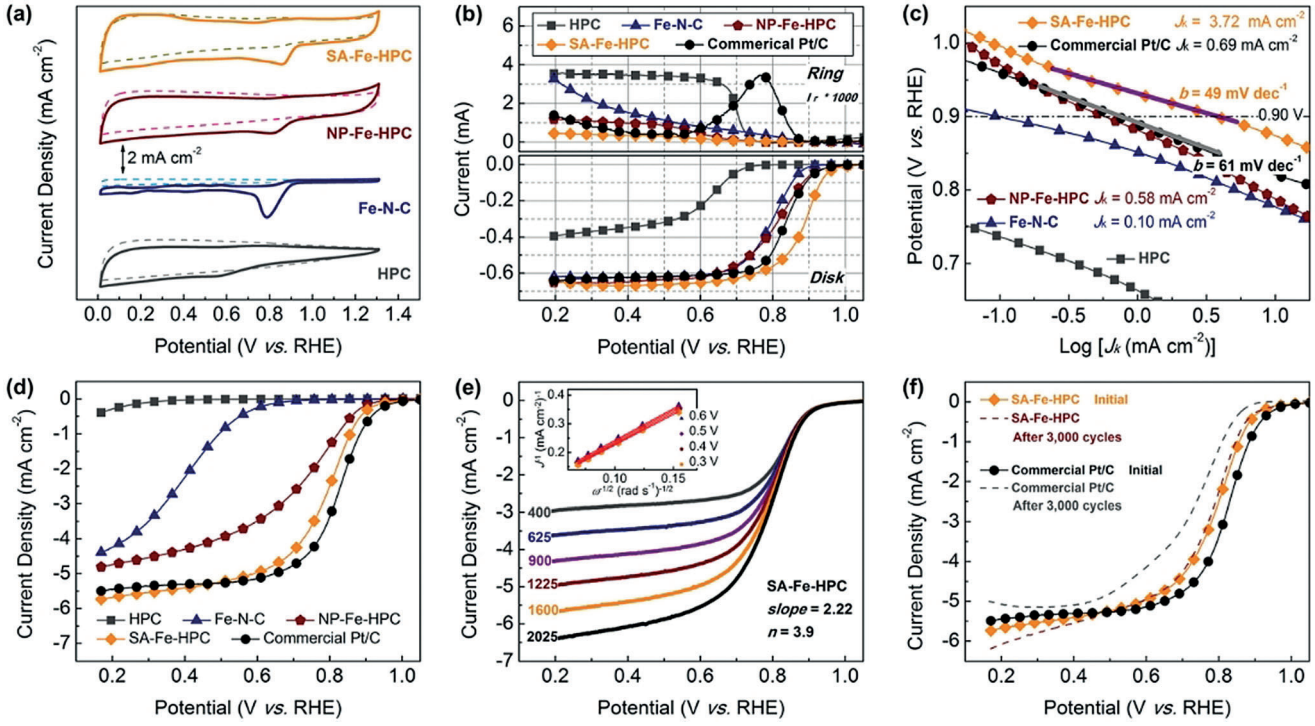

Figure 3. a) CV curves of HPC, Fe-N-C, NP-Fe-HPC, and SA-Fe-HPC in O_2-saturated (solid line) or N_2-saturated (dashed line) in 0.1 M KOH at a sweep rate of 50 mV s^{-1}. b) The corresponding RRDE voltammograms recorded in O_2-saturated 0.1 M KOH at 1600 rpm. The disk potential was scanned at 5 mV s^{-1}, and the ring potential was constant at 1.5 V. c) Tafel plots derived by the mass-transport correction from the corresponding LSV data. d) LSV voltammograms recorded in O_2-saturated 0.1 M H_2SO_4 at 1600 rpm with a sweep rate of 5 mV s^{-1}. e) LSV polarization curves of the SA-Fe-HPC electrode in O_2-saturated 0.1 M H_2SO_4 at a sweep rate of 5 mV s^{-1} with the different rotation rates (400–2025 rpm). The inset in (e) shows corresponding K-L plots (J^{-1} versus $\omega^{-1/2}$) at different potentials. f) ORR polarization curves of SA-Fe-HPC and Pt/C before and after 3000 potential cycles over 0.6–1.1 V with the sweep rate of 100 mV s^{-1} in N_2-saturated 0.1 M H_2SO_4.

FePc (1.6 Å), arising from the strong interaction between Fe and N atoms associated with the axial-coordinated N-ligands.[5b,11b,25] In contrast to the pronounce Fe-Fe bonding peak observed in Figure 2b for the NP-Fe-HPC. The absence of Fe–Fe paths (2.2 Å) in the SA-Fe-HPC indicates unambiguously that Fe atoms are in the single-atomic dispersion without the metallic Fe^0 nanoparticle. Furthermore, we performed ^{57}Fe Mössbauer transmission spectroscopy to identify the different chemical states of iron in the SA-Fe-HPC and NP-Fe-HPC samples (Table S5). In Figure 2c, the Mössbauer spectrum of SA-Fe-HPC was deconvoluted into two doublets (D1 and D2), attributable to Fe-N_x complexes with Fe atoms in a low- and medium-spin state, respectively. However, the Mössbauer spectrum of NP-Fe-HPC exhibits a singlet, a doublet and two sextets corresponding to γ-Fe, ε-Fe_xN ($x \leq 2.1$), and α-iron/iron carbide, respectively.[12a,26] Thus, the absence of the singlet and sextet components for SA-Fe-HPC indicates that the SA-Fe-HPC is free from inorganic Fe- phases (i.e., α-/γ-Fe,). These experimental data are further supported by density functional theory (DFT) calculations (see, Figures S11 and S12 in the Supporting Information for details).

To evaluate the ORR catalytic activity of SA-Fe-HPC, we first conducted cyclic voltammetric (CV) measurements for SA-Fe-HPC in N_2- and O_2-saturated alkaline electrolytes (0.1M KOH, Figure 3a). As can be seen, all the Fe-based electrodes displayed a well-defined catholic ORR peak at potentials between 0.75 and 0.90 V (vs. reversible hydrogen electrode (RHE), the same below) in the O_2-saturated 0.1M KOH solution, but not in the N_2-saturated solution. Among them, the SA-Fe-HPC electrode showed the highest catalytic activity with the most positive ORR peak potential and the strongest cathodic current. Also, the linear sweep voltammetry (LSV) curves recorded on the rotating ring-disk electrode (RRDE) in O_2-saturated 0.1M KOH (Figure 3b, bottom and Figure S14) showed that the SA-Fe-HPC electrode exhibited the best ORR performance with the most positive half-wave potential ($E_{1/2}$) of 0.89 V and the highest diffusion limited current density (J_d) of 5.4 mA cm^{-2} among all the electrodes investigated in this study (HPC, $E_{1/2} = 0.63$ V, $J_d = 2.8$ mA cm^{-2}; NP-Fe-HPC, $E_{1/2} = 0.82$ V, $J_d = 5.2$ mA cm^{-2}; Fe-N-C, $E_{1/2} = 0.80$ V, $J_d = 5.0$ mA cm^{-2}), and even much better than that of the commercial Pt/C ($E_{1/2} = 0.84$ V, $J_d = 5.0$ mA cm^{-2}). As expected, the SA-Fe-HPC electrode also displayed the lowest ring current (Figure 3b, top). Figure 3c shows the corresponding Tafel curves and kinetic currents (J_k) at 0.90 V with the mass-transport correction. Once again, the SA-Fe-HPC electrode exhibited the highest J_k (3.72 mA cm^{-2}), which is 5.4-fold higher than that of the commercial Pt/C, and a smaller Tafel slope (49 mV dec^{-1}) even than that of the Pt/C electrode (61 mV dec^{-1}) in the low over-potential region, indicating that the SA-Fe-HPC is an efficient electrocatalyst—even better than the commercial Pt/

C catalyst. As shown in Figure S15 and S16a, The SA-Fe-HPC showed a direct 4-electron transfer pathway for ORR.

It was further found that the acidic ORR performance followed the same trend as in the alkaline electrolyte (vide supra) with the catalytic activity increased in the following order: Fe-N-C < NP-Fe-HPC < SA-Fe-HPC (Figure S17). Figure 3d shows the corresponding LSV curves recorded in O_2-satured 0.1M H_2SO_4, which still shows a significantly higher ORR activity ($E_{1/2} = 0.81$ V, $J_d = 5.5$ mA cm^{-2}) for SA-Fe-HPC than those of HPC, NP-Fe-HPC ($E_{1/2} = 0.75$ V, $J_d = 4.6$ mA cm^{-2}) and Fe-N-C ($E_{1/2} = 0.39$ V), and even comparable to the commercial Pt/C catalyst ($E_{1/2} = 0.84$ V, $J_d = 5.5$ mA cm^{-2}). This could be attributed to a synergetic effect associated with the high concentration of active sites and the efficient mass transfer through the 3D porous structure.[9,14] The electron transfer number of SA-Fe-HPC in acidic electrolyte was calculated from the K-L plots at various potentials (Figure 3e) to be 4, indicating a direct 4-electron transfer pathway as for the commercial Pt/C (Figure S16b).

Finally, the SA-Fe-HPC electrode was found to be remarkably stable in the harsh oxygen reducing environment (Figures 3f, S18, and S19) and almost free from the methanol-crossover effect in both alkaline and acidic electrolytes (Figure S20), having a much better fuel selectivity than that of the commercial Pt/C. Unlike the easy demetalation and/or degradation of FePc molecules, the enhanced interaction between Fe atoms and the carbon support in SA-Fe-HPC stabilized the Fe atom at its active site, especially in the acidic environment.[9,17] Therefore, the SA-Fe-HPC catalyst is of great potential as a Pt substituent for practical applications.

In conclusion, we have developed a general strategy to prepare a Fe-based catalyst with atomic Fe dispersion on a porous carbon support, which has been demonstrated to show excellent performance for ORR in both alkaline and acidic electrolytes, making it a promising candidate to replace Pt-based ORR catalysts even for PEM fuel cells. The remarkable ORR performance of the SA-Fe-HPC is attributable to the well-defined dispersion of single Fe atomic active sites with an optimized coordination environment of Fe atoms on a 3D hierarchical porous carbon support with a high concentration/exposure of active sites. The methodology developed in this study could be used for producing various high-performance single-atom catalysts from earth abundant biomasses and metal complexes.

Acknowledgements

This work was supported by the National Natural Science Funds of China (51432003, 51125007, 51732002) and the International Joint Graduate-Training Program of BUCT. We are thankful to the beamline 1W1B station of Beijing Synchrotron Radiation Facility for the XAFS tests.

Conflict of interest

The authors declare no conflict of interest.

Keywords: electrocatalysis · hierarchical porous carbon · iron · oxygen reduction reaction (ORR) · single-atom catalysts

[1] a) L. Dai, Y. Xue, L. Qu, H. J. Choi, J. B. Baek, *Chem. Rev.* **2015**, *115*, 4823 – 4892; b) Z. W. Seh, J. Kibsgaard, C. F. Dickens, I. Chorkendorff, J. K. Nørskov, T. F. Jaramillo, *Science* **2017**, *355*, 146; c) M. Shao, Q. Chang, J. Dodelet, R. Chenitz, *Chem. Rev.* **2016**, *116*, 3594 – 3657; d) A. A. Gewirth, J. A. Varnell, A. M. DiAscro, *Chem. Rev.* **2018**, *118*, 2313 – 2339.

[2] M. Winter, R. J. Brodd, *Chem. Rev.* **2004**, *104*, 4245 – 4269.

[3] a) R. Borup, J. Meyers, B. Pivovar, *Chem. Rev.* **2007**, *107*, 3904 – 3951; b) X. Huang, Z. Zhao, L. Cao, Y. Chen, E. Zhu, Z. Lin, M. Li, A. Yan, A. Zettl, Y. M. Wang, X. Duan, T. Mueller, Y. Huang, *Science* **2015**, *348*, 1230 – 1234; c) M. Li, Z. Zhao, T. Cheng, A. Fortunelli, C. Y. Chen, R. Yu, Q. Zhang, L. Gu, B. V. Merinov, Z. Lin, E. Zhu, T. Yu, Q. Jia, J. Guo, L. Zhang, W. A. Goddard, Y. Huang, X. Duan, *Science* **2016**, *354*, 1414 – 1419; d) Y. Nie, L. Li, Z. Wei, *Chem. Soc. Rev.* **2015**, *44*, 2168 – 2201.

[4] a) C. Sealy, *Mater. Today* **2008**, *11*, 65 – 68; b) B. C. H. Steele, A. Heinzel, *Nature* **2001**, *414*, 345 – 352.

[5] a) Y. C. Wang, Y. J. Lai, L. Song, Z. Y. Zhou, J. G. Liu, Q. Wang, X. D. Yang, C. Chen, W. Shi, Y. P. Zheng, M. Rauf, S. G. Sun, *Angew. Chem. Int. Ed.* **2015**, *54*, 9907 – 9910; *Angew. Chem.* **2015**, *127*, 10045 – 10048; b) R. Cao, R. Thapa, H. Kim, X. Xu, M. G. Kim, Q. Li, N. Park, M. Liu, J. Cho, *Nat. Commun.* **2013**, *4*, 2076; c) G. Wu, K. L. More, C. M. Johnston, P. Zelenay, *Science* **2011**, *332*, 443 – 447.

[6] a) W. Xia, A. Mahmood, Z. Liang, R. Zou, S. Guo, *Angew. Chem. Int. Ed.* **2016**, *55*, 2650 – 2676; *Angew. Chem.* **2016**, *128*, 2698 – 2726; b) V. Georgakilas, J. N. Tiwari, K. C. Kemp, J. A. Perman, A. B. Bourlinos, K. S. Kim, R. Zboril, *Chem. Rev.* **2016**, *116*, 5464 – 5519.

[7] a) A. B. Sorokin, *Chem. Rev.* **2013**, *113*, 8152 – 8191; b) A. Morozan, B. Jousselme, S. Palacin, *Energy Environ. Sci.* **2011**, *4*, 1238 – 1254.

[8] a) W. Li, A. Yu, C. H. Drew, G. L. Bernard, Z. Chen, *J. Am. Chem. Soc.* **2010**, *132*, 17056 – 17058; b) Z. Zhang, S. Yang, M. Dou, H. Liu, L. Gu, F. Wang, *RSC Adv.* **2016**, *6*, 67049 – 67056.

[9] J. Shui, M. Wang, F. Du, L. Dai, *Sci. Adv.* **2015**, *1*, e1400129.

[10] X. F. Yang, A. Wang, B. Qiao, J. Li, J. Liu, T. Zhang, *Acc. Chem. Res.* **2013**, *46*, 1740 – 1748.

[11] a) H. J. Qiu, Y. Ito, W. Cong, Y. Tan, P. Liu, A. Hirata, T. Fujita, Z. Tang, M. Chen, *Angew. Chem. Int. Ed.* **2015**, *54*, 14031 – 14035; *Angew. Chem.* **2015**, *127*, 14237 – 14241; b) P. Yin, T. Yao, Y. Wu, L. Zheng, Y. Lin, W. Liu, H. Ju, J. Zhu, X. Hong, Z. Deng, G. Zhou, S. Wei, Y. Li, *Angew. Chem. Int. Ed.* **2016**, *55*, 10800 – 10805; *Angew. Chem.* **2016**, *128*, 10958 – 10963; c) W. Liu, L. Zhang, W. Yan, X. Liu, X. Yang, S. Miao, W. Wang, A. Wang, T. Zhang, *Chem. Sci.* **2016**, *7*, 5758 – 5764; d) H. Fei, J. Dong, M. J. Arellano-Jimenez, G. Ye, N. Dong Kim, E. L. Samuel, Z. Peng, Z. Zhu, F. Qin, J. Bao, M. J. Yacaman, P. M. Ajayan, D. Chen, J. M. Tour, *Nat. Commun.* **2015**, *6*, 8668; e) S. Yang, J. Kim, Y. J. Tak, A. Soon, H. Lee, *Angew. Chem. Int. Ed.* **2016**, *55*, 2058 – 2062; *Angew. Chem.* **2016**, *128*, 2098 – 2102.

[12] a) A. Zitolo, V. Goellner, V. Armel, M. T. Sougrati, T. Mineva, L. Stievano, E. Fonda, F. Jaouen, *Nat. Mater.* **2015**, *14*, 937 – 942; b) W. J. Jiang, L. Gu, L. Li, Y. Zhang, X. Zhang, L. J. Zhang, J. Q. Wang, J. S. Hu, Z. Wei, L. J. Wan, *J. Am. Chem. Soc.* **2016**, *138*, 3570 – 3578; c) Z. Qiao, H. Zhang, S. Karakalos, S. Hwang, J. Xue, M. Chen, D. Su, G. Wu, *Appl. Catal. B* **2017**, *219*, 629 – 639; d) X. Wang, H. Zhang, H. Lin, S. Gupta, C. Wang, Z. Tao, H. Fu, T. Wang, J. Zheng, G. Wu, X. Li, *Nano Energy* **2016**, *25*, 110 – 119; e) H. Zhang, S. Hwang, M. Wang, Z. Feng, S. Karakalos, L. Luo, Z. Qiao, X. Xie, C. Wang, D. Su, Y. Shao, G. Wu, *J. Am.*

Chem. Soc. **2017**, *139*, 14143 – 14149; f) X.-X. Wang, D.-A. Cullen, Y.-T. Pan, S. Hwang, M. Wang, Z. Feng, J. Wang, M.-H. Engelhard, H. Zhang, Y. He, Y. Shao, D. Su, K.-L. More, J.-S. Spendelow, G. Wu, *Adv. Mater.* **2018**, *30*, 1706758.

[13] a) Z. K. Yang, L. Lin, A. W. Xu, *Small* **2016**, *12*, 5710 – 5719; b) L. Lin, Q. Zhu, A. W. Xu, *J. Am. Chem. Soc.* **2014**, *136*, 11027 – 11033.

[14] S. Yasuda, A. Furuya, Y. Uchibori, J. Kim, K. Murakoshi, *Adv. Funct. Mater.* **2016**, *26*, 738 – 744.

[15] a) P. J. Wei, G. Q. Yu, Y. Naruta, J. G. Liu, *Angew. Chem. Int. Ed.* **2014**, *53*, 6659 – 6663; *Angew. Chem.* **2014**, *126*, 6777 – 6781; b) Z. Zhang, M. Dou, J. Ji, F. Wang, *Nano Energy* **2017**, *34*, 338 – 343.

[16] H. Tang, H. Yin, J. Wang, N. Yang, D. Wang, Z. Tang, *Angew. Chem. Int. Ed.* **2013**, *52*, 5585 – 5589; *Angew. Chem.* **2013**, *125*, 5695 – 5699.

[17] a) Z. Zhang, X. Gao, M. Dou, J. Ji, F. Wang, *J. Mater. Chem. A* **2017**, *5*, 1526 – 1532; b) M. Sumimoto, Y. Kawashima, K. Horia, H. Fujimoto, *Dalton Trans.* **2009**, 5737 – 5746.

[18] a) M. M. Titirici, R. J. White, N. Brun, V. L. Budarin, D. S. Su, F. del Monte, J. H. Clark, M. J. MacLachlan, *Chem. Soc. Rev.* **2015**, *44*, 250 – 290; b) M. Dou, D. He, W. Shao, H. Liu, F. Wang, L. Dai, *Chem. Eur. J.* **2016**, *22*, 2896 – 2901.

[19] a) J. L. Oberst, M. S. Thorum, A. A. Gewirth, *J. Phys. Chem. C* **2012**, *116*, 25257 – 25261; b) M. S. Thorum, J. M. Hankett, A. A. Gewirth, *J. Phys. Chem. Lett.* **2011**, *2*, 295 – 298; c) V. Bambagioni, C. Bianchini, J. Filippi, A. Lavacchi, W. Oberhauser, A. Marchionni, S. Moneti, F. Vizza, R. Psaro, V.-D. Santo, A. Gallo, S. Recchia, L. Sordelli, *J. Power Sources* **2011**, *196*, 2519 – 2529; d) M. Li, X. Bo, Y. Zhang, C. Han, L. Guo, *J. Power Sources* **2014**, *264*, 114 – 122.

[20] a) J. Guan, Z. Zhang, J. Ji, M. Dou, F. Wang, *ACS Appl. Mater. Interfaces* **2017**, *9*, 30662 – 30669; b) Z. Zhang, X. Gao, M. Dou, J. Ji, F. Wang, *Small* **2017**, *13*, 1604290.

[21] a) S. Gao, H. Liu, K. Geng, X. Wei, *Nano Energy* **2015**, *12*, 785 – 793; b) S. Gao, X. Wei, H. Fan, L. Li, K. Geng, J. Wang, *Nano Energy* **2015**, *13*, 518 – 526.

[22] a) J. Zhang, Z. Zhao, Z. Xia, L. Dai, *Nat. Nanotechnol.* **2015**, *10*, 444 – 452; b) Z. Zhang, M. Dou, H. Liu, L. Dai, F. Wang, *Small* **2016**, *12*, 4193 – 4199.

[23] T. E. Westre, P. Kennepohl, J. G. DeWitt, B. Hedman, K. O. Hodgson, E. I. Solomon, *J. Am. Chem. Soc.* **1997**, *119*, 6297 – 6314.

[24] a) W.-F. Chen, S. Iyer, S. Iyer, K. Sasaki, C.-H. Wang, Y. Zhu, J. T. Muckerman, E. Fujita, *Energy Environ. Sci.* **2013**, *6*, 1818 – 1826; b) W. F. Chen, C. H. Wang, K. Sasaki, N. Marinkovic, W. Xu, J. T. Muckerman, Y. Zhu, R. R. Adzic, *Energy Environ. Sci.* **2013**, *6*, 943 – 951; c) Z. L. Wang, X. F. Hao, Z. Jiang, X. P. Sun, D. Xu, J. Wang, H. X. Zhong, F. L. Meng, X. B. Zhang, *J. Am. Chem. Soc.* **2015**, *137*, 15070 – 15073.

[25] T. Li, Y. Peng, K. Li, R. Zhang, L. Zheng, D. Xia, X. Zuo, *J. Power Sources* **2015**, *293*, 511 – 518.

[26] U. I. Kramm, M. Lefevre, N. Larouche, D. Schmeisser, J. P. Dodelet, *J. Am. Chem. Soc.* **2014**, *136*, 978 – 985.

Manuscript received: April 27, 2018
Version of record online: ■■ ■■, ■■■■

Communications

Oxygen Reduction Reaction

Z. Zhang, J. Sun, F. Wang,*
L. Dai* ——— ■■■■–■■■■

Efficient Oxygen Reduction Reaction (ORR) Catalysts Based on Single Iron Atoms Dispersed on a Hierarchically Structured Porous Carbon Framework

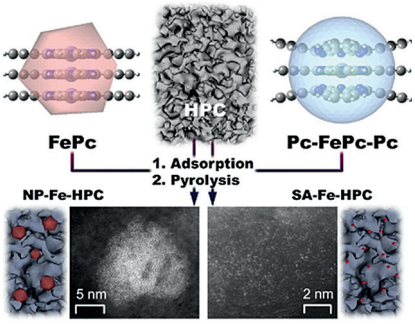

Stay single: Single-atom catalysts with Fe atoms dispersed on hierarchical porous carbons were prepared by pyrolysis of iron phthalocyanine and unsubstituted phthalocyanine complexes confined within micropores of the porous carbon supports. The resulting catalysts outperformed the commercial Pt/C electrode in alkaline electrolytes and showed an electrocatalytic activity comparable to the commercial Pt/C electrode in acidic media with a better long-term stability.